2011 IEEE International Conference on Robotics and Automation
Shanghai International Conference Center
May 9-13, 2011, Shanghai, China

A Distributed Model for Needle-Tissue Friction in Percutaneous Interventions

Ali Asadian, Rajni V. Patel, and Mehrdad R. Kermani.

Abstract— **This paper presents a new approach to account for distributed friction in needle insertion in soft tissue. As is well known, friction is a complex nonlinear phenomenon, and it appears that classical or static models are unable to capture some of the observations in systems subject to significant frictional effects. To characterize dynamic features when the needle is very flexible and friction plays an important role in bending mechanics or when a stop-and-start planning scenario is implemented at low insertion velocities, a distributed LuGre model can be adopted. Experimental results using an artificial phantom illustrate that the proposed method is capable of representing the main features of friction which is a major force component in needle-tissue interaction during percutaneous interventions.**

I. Introduction

The use of flexible needles in percutaneous interventions can facilitate curved trajectories which are beneficial for localized drug delivery, radioactive seed placement, and biopsy especially when target points are difficult to access. However, needle misplacement can degrade the effectiveness of the treatment or can lead to misdiagnosis. Therefore, accurate needle-tip placement is very important in many therapeutic procedures, and robot-assisted needle steering, whose function is to steer the needle to specific targets inside soft tissue, has become an active research area [1].

In order to design a proper control strategy, interaction between the needle and living tissue that has a complex behavior has to be thoroughly studied. In this context, pre-puncture corresponds to viscoelastic behavior while complex force behavior during post-puncture or insertion phase stems from the combined effects of cutting force, friction, and skin relaxation. Finally, during retraction or needle withdrawal, friction is the sole interaction force. As is known, friction as an inevitable physical phenomenon plays a central controlling role in diverse applications, and research on systems with friction has a long and rich history [2]. Friction occurs in mechanisms where bodies in contact have relative motion, and causes the performance of servomechanisms to deteriorate and results in undesirable behaviors such as tracking errors. The undesirable impacts are affected by temperature, material of the contact surfaces, and lubrication.

A. Asadian, R.V. Patel, and M.R. Kermani are with Canadian Surgical Technologies and Advanced Robotics (CSTAR), Lawson Health Research Institute, and the Department of Electrical and Computer Engineering, The University of Western Ontario, London, Ontario, Canada, aasadian@uwo.ca, rvpatel@uwo.ca, mkermani@eng.uwo.ca

R.V. Patel is also with the Department of Surgery, The University of Western Ontario, London, Ontario, Canada

In our application, to steer a flexible needle, the needle is likely to stop and rotate before further insertions [3]–[5]. This specific steering strategy introduces a sequence of low-velocity start-and-turn motions and switches the needle status between pre-sliding and sliding regimes. We formulate a model of translational friction that investigates the dynamic behavior of distributed friction along the contact patch when the needle interacts with an elastic medium. In particular, when the needle is very flexible or it is subject to consecutive stops and starts at low insertion velocities, the corresponding impact may be significant.

In the future, adding the frictional effects as developed in this paper to the preliminary beam models [4], [6], and then incorporating the resultant bending mechanism into path planners [3], [5] are expected to provide a better steering accuracy. It is the main motivation of the present work. The remainder of this paper is organized as follows. Section II briefly reviews modeling studies regarding needle-tissue interaction, and highlights the lack of an appropriate analytical model for distributed friction in minimally invasive surgery. In section III, the proposed methodology to include the effect of friction in our application is described. Section IV, presents a short description of our setup followed by simulation results and experimental tests performed to evaluate our work. Finally, section V draws conclusions and suggests future work.

II. Related Work

Different studies have been performed dealing with the measurement and the modeling of forces involved in percutaneous needle insertion. However, the authors believe that the complexity of the mechanism of friction in needle insertion deserves further detailed examinations.

As a pioneering work for force modeling in minimally invasive surgery, Okamura et al. [7] proposed an empirical model for bilateral needle-tissue insertion force, which was a summation of capsule stiffness force, friction and cutting forces. Accordingly, the stiffness force occurs before the puncture of the capsule while the friction and cutting force occur right after the main puncture. In this study, the friction force was described by a modified Karnopp model, which was comprised of a viscous term plus a constant static friction within a dead zone in the vicinity of zero. Kataoka et al. [8] measured the forces and analyzed them qualitatively without any explicit quantification. Barbe et al. [9] developed an on-line scheme using recursive least-squares with covariance resetting to characterize force evolution during needle insertion. They integrated this estimator with

978-1-61284-385-8/11/$26.00 ©2011 IEEE

the Kelvin-Voigt (KV) viscoelastic interaction model, and proposed a statistical method to detect rupture. According to their analysis and possibly due to ignoring friction, an accurate biomechanical model cannot be estimated in an online manner. Abolhassani and Patel [4], [6] ignored the vertical component of stick-slip friction along the insertion depth and solved the bending-moment equation in the static regime toward steering a flexible needle. However, this assumption is not realistic when the needle is very flexible, or stiction is important. Webster et al. [10] developed a kinematic model for steering a flexible bevel-tip needle in relatively stiff rubber. Accordingly, the needle tip acts like a small bicycle with locked handlebars while it moves along an arc of approximately fixed radius. In this model, distributed friction and tissue deformation were neglected although they could have a considerable impact.

In summary, the essence of our work comes from the method developed by Canudas et al. [12]. They presented a LuGre-based dynamic model for the longitudinal road-tire interaction for wheeled ground vehicles, and developed a partial differential equation (PDE) for friction distribution along a fixed patch. Parameters of this model, which are velocity-dependent, are used to capture the contact characteristics. Referring to this work, in the current study our goal is to develop a solution that is applicable to needle insertion, and incorporates the effect of instantaneous velocity in the estimation. We have analyzed and modeled the dynamic behavior of the distributed friction that can potentially play an important role in bending mechanics during discrete insertions. In our case, as opposed to the road-tire problem, contact area changes with respect to time, and toward our goal, an approximate lumped form makes the distributed LuGre model more suitable for the development and implementation of an identification algorithm.

III. Proposed Modeling Scheme

Several studies have explored different aspects of friction, and numerous models have been developed to account for it [2], [11]–[15]. Despite its complexity, it has been recognized that two important ingredients are always present in the current models that generate a force against motion: Coulomb and viscous friction. There exist other interesting properties observed in systems with friction such as stick-slip motion, pre-sliding displacement, Dahl effect and frictional lag that cannot be explained only by static models. This is basically due to the fact that friction does not have an instantaneous response, but has internal dynamics. That is why dynamic models such as the LuGre model have been widely discussed in the literature [2], [11], [12], and have been extensively applied to robotics applications [14], [15].

The LuGre model is able to capture the aforementioned complex features, and is therefore discussed in this section as a basis for our study. The point friction model [2], [11] can be extended to a distributed version [12] along the inserted portion of the needle by letting $z(\zeta,t)$ denote the model's internal state or the deflection of the bristle elements located at the point ζ at a certain time t. The model is therefore

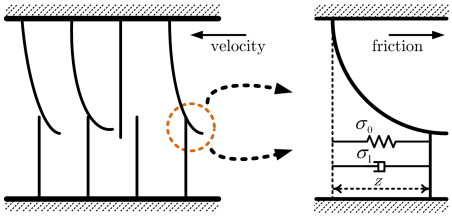

Fig. 1. Microscopic representation of irregular contact surfaces and elastic bristles whose bending gives rise to the friction force

written as follows

$$\begin{cases} \frac{dz}{dt}(\zeta,t) = v - \frac{\sigma_0|v|}{g(v)}z \\ F_{friction}(t) = \int_0^{L(t)} dF(\zeta,t) \end{cases} \tag{1}$$

$$g(v) = \mu_c + (\mu_s - \mu_c)e^{-\alpha|v|} \tag{2}$$

where v is the contact velocity of each differential element and L is the incision length; and

$$dF(\zeta,t) = \{\sigma_0 z(\zeta,t) + \sigma_1 \frac{\partial z}{\partial t}(\zeta,t) + \sigma_2 v\} dF_n(\zeta,t) \tag{3}$$

As observed, the total force is characterized by four static parameters namely μ_c, μ_s, σ_2, and α and two dynamic parameters: σ_0 and σ_1. σ_0 can be understood as being the stiffness coefficient of the microscopic deformations during the pre-sliding displacement, and σ_1 as being the damping coefficient associated with $\dot{z}$. σ_2 is the viscous relative damping while μ_c and μ_s are the normalized Coulomb and stiction friction, respectively. Also, the function g yields the classical Stribeck effect. Herein, $dF(\zeta,t)$ is the differential friction force developed in the element $d\zeta$, and $dF_n(\zeta,t)$ is the differential normal force applied to the same element at time t. Fig. 1 helps us to get more insight into this model which is based on the deflection of spring-like bristles that exists at the microscopic level of two moving surfaces.

Assuming a steady-state normal force distribution and introducing a normal force density function $f_n(\zeta)$ (force per unit length) along the patch as shown in Fig. 2, we have

$$dF_n(\zeta,t) = dF_n(\zeta) = f_n(\zeta)d\zeta \tag{4}$$

By substitution, the tangential friction force is given by

$$F_{friction}(t) = \int_0^{L(t)} \{\sigma_0 z(\zeta,t) + \sigma_1 \frac{\partial z}{\partial t}(\zeta,t) + \sigma_2 v\} f_n(\zeta) d\zeta \tag{5}$$

The friction force acts on the side wall of the needle shaft in the axial direction while the clamping force is applied in the normal direction. The latter force is the impact of tissue resistance, and is affected by the incision shape created by the needle tip, as well as the needle size. The cutting force is also modeled as a single force placed at the tip. Setting

$$\frac{dz}{dt}(\zeta,t) = \frac{\partial z}{\partial \zeta}\frac{\partial \zeta}{\partial t} + \frac{\partial z}{\partial t} \tag{6}$$

in (1) and $\frac{\partial \zeta}{\partial t} = v$ render the following PDE that has to be solved in time and space to find a closed-form solution for the friction model:

$$\frac{\partial z}{\partial \zeta}(\zeta,t) = 1 - sign(v)\frac{\sigma_0}{g(v)}z - \frac{1}{v}\frac{\partial z}{\partial t}(\zeta,t) \tag{7}$$

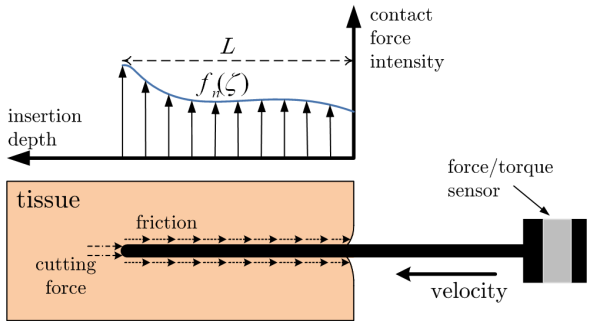

Fig. 2. Needle-tissue interaction and involved force components

Assuming the deflection of the first bristle element to be zero imposes the boundary condition as $z(0,t)=0$ for $\forall t \geq 0$. In a quasi-static condition where $\frac{\partial z}{\partial t}(\zeta,t) \simeq 0$ within a small enough interval of time, we obtain

$$\frac{\partial z}{\partial \zeta}(\zeta,t) = 1 - sign(v)\frac{\sigma_0}{g(v)}z \quad \zeta \in (0,L) \tag{8}$$

The solution of the ordinary differential equation (ODE) defined by (8) is expressed as follows, and can approximate the solution of the PDE introduced in (7). It is assumed here that the bristles have a faster dynamic response compared to variations of the insertion velocity.

$$z_{qs} = \frac{g(v)}{\sigma_0}(1 - e^{-\frac{\sigma_0}{g(v)}\zeta})sign(v) \tag{9}$$

$$F_{qs} = \int_0^L \{\sigma_0 z_{qs} + \sigma_2 v\} f_n(\zeta) d\zeta \tag{10}$$

To calculate the steady-state solution of the friction, it is required to know the distribution for the force density function. For the sake of simplicity, we presume a uniform load where $f_n(\zeta) = F_n/L$ for $\zeta \in (0,L)$. This assumption agrees with the estimated force density along the needle shaft as reported in [16]. Here, F_n denotes the total normal load along the shaft. Therefore, we have

$$F_{qs} = \Big(sign(v)g(v)\big[1 - \frac{g(v)}{\sigma_0 L}(1 - e^{-\frac{\sigma_0 L}{g(v)}})\big] + \sigma_2 v\Big)F_n \tag{11}$$

Following this strategy and fitting the steady-state representation of equation (1) to experimental data, the unknown parameters except σ_1 can be identified. As another numerical approach that is proposed in this paper, it is notable that the distributed model introduced by (1) is in agreement with a lumped model in the following sense: let us assume that the patch region does not change with respect to time, i.e., $\frac{dL}{dt}(t) = 0$, and the force distribution is uniform. A mean friction state is defined as

$$\tilde{z}(t) = \frac{1}{F_n}\int_0^L z(\zeta,t) f_n(\zeta) d\zeta \tag{12}$$

Using (7) and doing a few manipulations [12], the new lumped model with respect to $\tilde{z}$ is given by

$$\begin{cases} \dot{\tilde{z}} = v - \Big(\frac{\sigma_0}{g(v)} - \kappa(t)\Big) \mid v \mid \tilde{z} \\ F_{friction}(t) = F_n(\sigma_0 \tilde{z} + \sigma_1 \dot{\tilde{z}} + \sigma_2 v) \end{cases} \tag{13}$$

where

$$\kappa(t) = \frac{1}{F_n \tilde{z}}\Big([z(\zeta,t)f_n(\zeta)]_0^L - \int_0^L z(\zeta,t)\frac{\partial f_n(\zeta)}{\partial \zeta} d\zeta\Big) \tag{14}$$

The first term on the right-hand side of (14) represents the effect of the boundary conditions while the term under the integral describes the impact of the force distribution. This approximation is called the average lumped model. Setting $\frac{\partial f_n}{\partial \zeta}(\zeta) = 0$ in the closed-form solution or equation (13) as a result of assuming a uniform load distribution with zero boundary conditions as

$$z(0,t)f_n(0) = z(L,t)f_n(L) = 0 \tag{15}$$

yields $\kappa(t) = 0$. This assumption is borrowed from the fact that a realistic solution, by continuity, provides zero normal force or zero bristle deflection at the boundaries of the contact area. In other words, a trapezoidal force profile that fully satisfies this constraint may be more realistically; however, the main reason for setting $f_n(\zeta)$ to be uniform along the shaft is to reduce the identification complexity. Thus,

$$\begin{cases} \dot{\tilde{z}} = v - \frac{\sigma_0 |v|}{g(v)}\tilde{z} \\ F_{friction}(t) = F_n(\sigma_0 \tilde{z} + \sigma_1 \dot{\tilde{z}} + \sigma_2 v) \end{cases} \tag{16}$$

This feasible scheme that is in fact the standard point-contact LuGre model will be used in the sequel for the purpose of identification.

IV. Instrumentation and Experimental Results

A. Experimental Setup

Experimental implementation of the proposed methodology is carried out on the state-of-the-art robotic system shown in Fig. 3 which has been fully designed and manufactured in our group specifically for the purpose of prostate brachytherapy [17]. The 5-DOF manipulator can perform orientation, insertion and rotation of the needle and linear motion of the plunger to drop radioactive seeds with an average RMS targeting error of 1.45mm. A Nano43 6-DOF force/torque sensor (ATI Industrial Automation) was attached to the needle holder, and the control computer and the data capture computer were interfaced through a UDP connection over ethernet. A multi-threaded application for real-time position/velocity control, sensor readings, and communication was developed using Microsoft® C++, MATLAB® and the QuaRC® Toolbox (Quanser Inc.). The robot is controlled using a PID controller at the rate of 1kHz while force/torque data are acquired at the rate of 200Hz after being smoothed by a moving average filter. This system is capable of implementing more advanced approaches; however, it was employed here to validate the proposed modeling scheme.

In this test-bed, the cannula of the 18Ga stainless steel needle (Cook Medical) has a cone tip with outer and inner diameters of 1.270mm and 0.838mm, respectively. Experiments were carried out on a Gelrite Gellan Gum (Sigma-Aldrich) with a concentration rate of 6% in water. Therefore, the tissue phantom is relatively stiff, and exhibits stick-slip behavior.

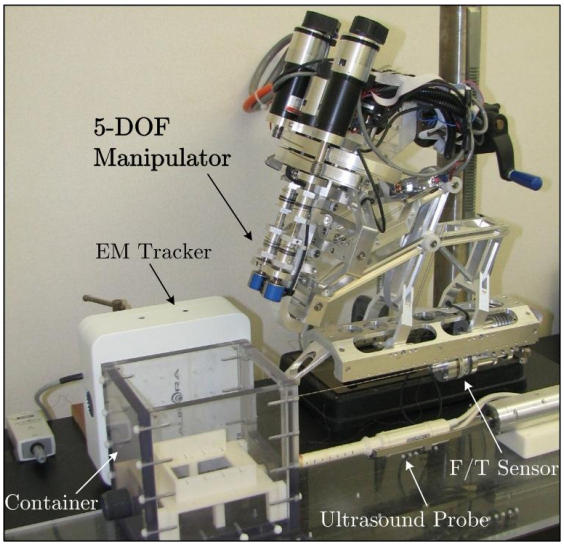

Fig. 3. A view of our robotic system

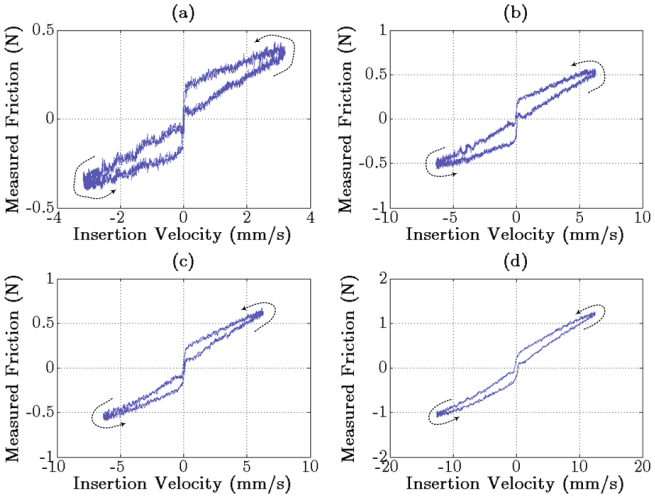

Fig. 4. Friction-velocity cycles: (a) f_{in}=0.025Hz and d_{in}=20mm (b) f_{in}=0.025Hz and d_{in}=40mm (c) f_{in}=0.05Hz and d_{in}=20mm (d) f_{in}=0.05Hz and d_{in}=40mm

B. Friction Identification

In order to further investigate friction, the following experiment was conducted. To excite the system in the axial direction, a low-frequency sinusoidal torque was applied to the last two joints of the robot. The frequency and the amplitude of this signal was selected so that it could transition the system from the pre-sliding to the sliding phase and vice versa. The proper selection required a few trials and errors that lead to a translational motion profile whose maximum amplitude (d_{in}) lies between 20mm and 40mm and its frequency (f_{in}) ranges from 0.02Hz to 0.1Hz. For identification, the needle was inserted into one side of the phantom with known thickness that was rigidly fixed to its container with the needle tip 5cm outside of the tissue. In this test, the tip was not cutting and there existed a constant amount of tissue in contact with the shaft; therefore, the force should be the same during insertion and retraction. The logged data was studied over 4 periodic cycles, and without loss of generality, F_n was set to 1 in the current study.

Note that the total axial force (F_z) measured by the F/T sensor is expressed as the sum of inertial and friction forces. The acceleration profile (a) and the mass of the needle plus its holder (m=46.55g) are known. Thus, we have

$$F_{friction}(measured) = F_z - ma \tag{17}$$

Clinical needle insertion rates usually vary between 0.4mm/s and 10mm/s [16]. Thus, to reduce noise perturbation that is dominant at low velocities which was the case in our experiments, a high-gain observer was implemented to estimate the velocity from encoder measurements. Given the velocity, another observer was then utilized to find the acceleration. In our implementation, it was observed that the estimated/measured friction-velocity cycles were highly affected by the observers' parameters particularly in the vicinity of the origin; therefore, the observers have to be carefully tuned. Fig. 4 demonstrates four sets of the empirical data used for identification. High noise level in a low-velocity profile, e.g., case (a), is essentially due to the existence of intricate friction in the internal structure of the robot which is too complex to be fully modeled and compensated for by the PID controller. As is apparent in this plot, the dynamic response of the friction is a function of the excitation frequency as well as its amplitude. The Stribeck effect is also visible at low insertion velocities.

TABLE I
ESTIMATED PARAMETERS OF THE PROPOSED MODEL

	d_{in}=20mm		d_{in}=40mm	
	f_{in}=0.025Hz	f_{in}=0.05Hz	f_{in}=0.025Hz	f_{in}=0.05Hz
σ_0	1.326	1.419	2.469	2.592
σ_1	1.423	1.312	0.845	0.879
σ_2	1.04×10^{-4}	0.001	2.76×10^{-4}	2.40×10^{-3}
μ_c	0.628	0.913	1.386	1.763
μ_s	0.045	0.033	0.084	0.052
α	0.256	0.152	0.079	0.075

Having obtained a friction-velocity map, the parameters of the model given in the previous section can be identified. More advanced studies and discussions have been reported in the literature on adaptive compensation and parameter identification of friction [13]–[15]. In the current study, we adopted the procedure followed by Kermani et al. [15] to identify the unknown parameters of our average lumped model (16), and repeated the same tests as described before at 5 different insertion points. Table I summarizes the averaged values of the estimated parameters. Statistical analysis is the subject of further research, and will be published in an extended version.

Figs. 5 and 6 present the estimated friction-velocity mappings as well as the experimental data for cases (a) and (c) as in Fig. 4. For comparison, the modified Karnopp model [7] was also implemented in this paper. We used the least-squares algorithm given in [7] to estimate the viscous and Coulomb coefficients. More details have been discussed in the same reference. This static model includes only viscous and Coulomb terms, and predicts the mapping

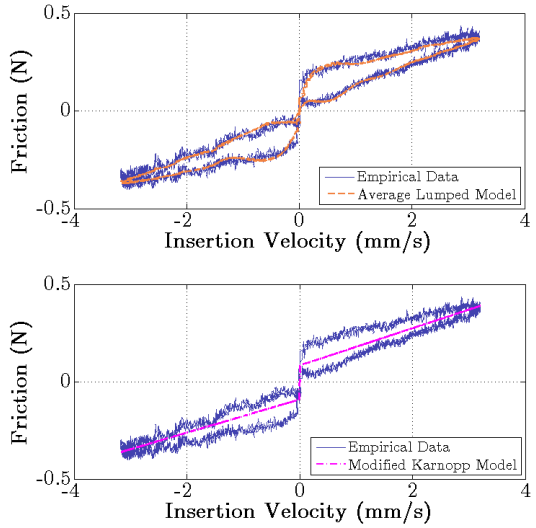

Fig. 5. Identified and experimental friction-velocity graph: f_{in}=0.025Hz and d_{in}=20mm

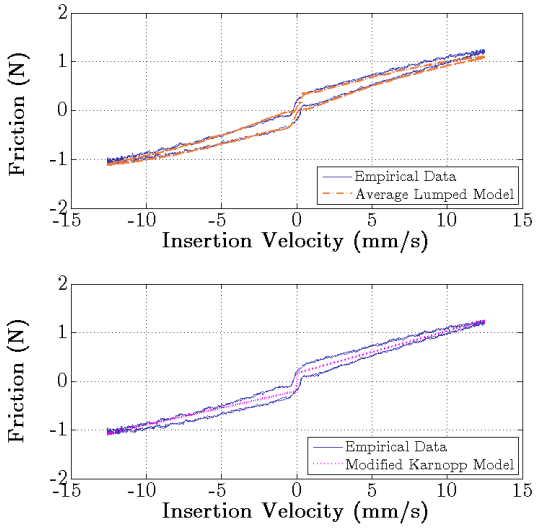

Fig. 6. Identified and experimental friction-velocity graph: f_{in}=0.05Hz and d_{in}=40mm

according to those in Figs. 5 and 6. The plots show that our proposed model is capable of capturing the dynamic behavior of friction including the Stribeck effect and the hysteresis loop during the intervention as opposed to the Karnopp model. The corresponding root mean squared error (RMSE) values of friction prediction in the four studied cases are also listed in Table II. The improvement achieved in terms of RMSE is at least 23%.

As is evident from the figures, the cycles are asymmetric stemming from the existence of possible perturbations during insertion. For example, a slight amount of cutting force may still be present in the forward motion in contrast to the backward retraction where friction is the sole interaction force. Here, a low-pass chebyshev filter was employed to remove high-frequency jitter from the estimations that is caused by the existing oscillations in the estimated velocities.

TABLE II
RMSE OF FRICTION FORCE PREDICTION (N)

	Proposed Model	Karnopp Model
d_{in}=20mm f_{in}=0.025Hz	0.0246	0.0479
d_{in}=40mm f_{in}=0.025Hz	0.0329	0.0644
d_{in}=20mm f_{in}=0.05Hz	0.0355	0.0461
d_{in}=40mm f_{in}=0.05Hz	0.0651	0.0855

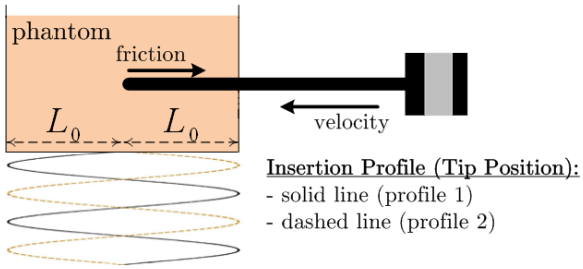

Fig. 7. Cyclic insertion profiles for friction estimation

C. Friction Estimation

Having identified the model, our next objective was to predict the behavior of the distributed friction along the incision line. To this end, the estimated values obtained from the approximate lumped model were fed into the distributed model to predict the friction behavior during an intra-operative test. The friction force is predicted using (1) and the identified values listed in Table I. To this end and due to the complexity of direct calculation of $F_{friction}(t)$, we used numerical approximations embedded in MATLAB® to integrate $dF(\zeta, t)$ in (1). We ran two tests in which f_{in} and d_{in} are respectively set to 0.05Hz and 40mm. The needle tip was initially placed in the middle point inside the phantom so that L_0=40mm. In the first profile illustrated in Fig. 7, the needle was first retracted until approaching the right wall of the container and then it was inserted toward the left wall. In the second profile, the tip motion had an opposite sequence.

Fig. 8 shows the estimated friction as well as the total measured interaction force during the first 50 seconds of the intervention. It is evident that the developed solution exhibits a reasonable accuracy except for the first negative lobes in both profiles. This should not come as a surprise since as observed, the empirical data does not follow an exact pattern throughout the entire simulation. Our model reflects only standard features of the friction phenomenon, e.g., viscous friction, hysteresis, and the Stribeck effect, and it does not justify discrepancies stemming from unmodeled dynamics.

In profile 1, within the first 5 seconds of motion, and in profile 2, from 10s to 15s, cutting occurs that is marked by asterisk signs. Possible extra cutting during cyclic insertions which has only a slight amount is ignored here. Note that in section IV-B, it was assumed that no cutting force was present while F_z in (17) denotes the summation of friction, cutting force, and inertial effect, in general. This means that during the aforementioned periods, the measured interaction

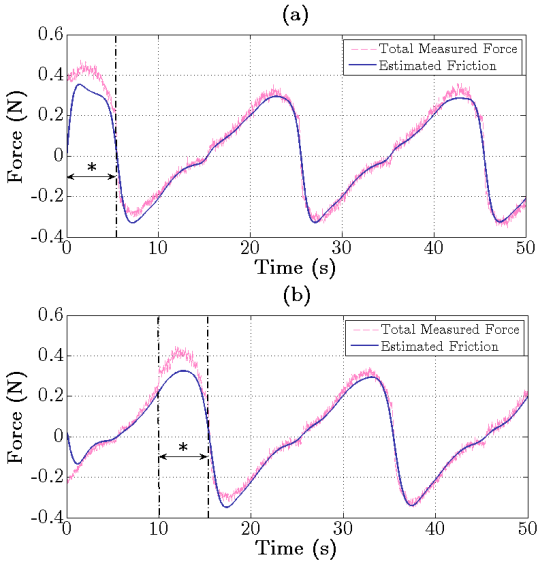

Fig. 8. Measured interaction force (cutting force + friction) and estimated friction: (a) profile 1 (b) profile 2

force equals the summation of the estimated friction and the cutting force. Therefore, we can take advantage of this approach to find an on-line estimation of the cutting force as well. However, care must be taken that due to the dynamics of the velocity observers and also embedded safety features in the manipulator's controller, it takes a few seconds for the estimator to track the actual velocity. This is the reason why the estimation is not accurate during the first few seconds of running the algorithm as shown in Fig. 8. Our approach cannot therefore be employed to predict the cutting force where the cutting region overlaps the inaccurate region as in Fig. 8(a).

Overall, the current match between the measured and the estimated forces presented in this paper proves the capability of our model to mimic and to deal with friction complexities. However, part of the conditions applied for the ease of identification, e.g., the presumed boundary conditions introduced by (15), made a perfect match impossible.

V. Concluding Remarks and Future Work

This paper presented a sophisticated approach to study and model complex features of friction during needle-tissue interaction in percutaneous interventions. The interaction between the needle and the tissue comprised a form of stick-slip friction, and our model was able to describe the dynamic behavior of the distributed friction along the needle shaft. A potential advantage of this scheme was its ability to capture parameters with physical interpretation such as the contact's stiffness and relative damping. In this study, due to the tip shape of the needle, bending was negligible, but future work will explore the effect of the distributed force on bending mechanics. To this end, the guidelines provided in this paper enable us to refine the static beam-based deflection models in which friction is ignored. Although not being very accurate, they are widely utilized for the purpose of steering due to their simplicity. Therefore, it is anticipated that friction integration in bending mechanism will significantly improve steering accuracy. At the very least, this work will need to be validated by *in vivo* percutaneous procedures which is part of our ongoing study.

VI. Acknowledgments

This research was supported by the Natural Sciences and Engineering Research Council (NSERC) of Canada under grants RGPIN-1345 (R.V. Patel) and RGPIN-346166 (M.R. Kermani). The development of the robotic system for prostate brachytherapy was supported by NSERC and CIHR (Canadian Institutes for Heath Research) under the Collaborative Health Research Projects Grant 262583-2003 (R.V. Patel, Principal Investigator).

References

[1] N. Abolhassani, R. Patel, and M. Moallem, Needle Insertion into Soft Tissue: A Survey, *Med. Eng. Phys.*, Vol. 29, pp. 413-431, 2007.

[2] H. Olsson, K.J. Astrom, C. Canudas De Wit, M. Gafvert, and P. Lichinsky, Friction Models and Friction Compensation, *Eur. J. Control*, vol. 4, no. 3, pp. 176-195, 1998.

[3] A. Asadian, M.R. Kermani, and R.V. Patel, "Accelerated Needle Steering Using Partitioned Value Iteration," *In Proc. of IEEE American Control Conference (ACC)*, USA, 2010, pp. 2785-2790.

[4] N. Abolhassani, R.V. Patel, and F. Ayazi, Minimization of Needle Deflection in Robot-Assisted Percutaneous Therapy, *Int. J. Med. Robotics Comput. Assist. Surg.*, vol. 3, pp. 140-148, 2007.

[5] V. Duindam, R. Alterovitz, S. Sastry, and K. Goldberg, "Screw-Based Motion Planning for Bevel-Tip Flexible Needles in 3D Environments with Obstacles," *In Proc. of IEEE Int. Conf. on Rob. Autom. (ICRA)*, USA, 2008, pp. 2483-2488.

[6] N. Abdolhassani, R.V. Patel, "Deflection of a Flexible Needle during Insertion into Soft Tissue," *In Proc. of 28th IEEE EMBS Annu. Int. Conf.*, USA, 2006, pp. 3858-3861.

[7] A.M. Okamura, C. Simone, and M.D. O'Leary, Force Modeling for Needle Insertion into Soft Tissue, *IEEE Trans. Biomed. Eng.*, vol. 51, pp. 1707-1716, 2004.

[8] H. Kataoka, T. Washio, K. Chinzei, K. Mizuhara, C. Simone, and A.M. Okamura, "Measurement of the Tip and Friction Force Acting on a Needle during Penetration," *In Proc. of 5th Int. Conf. on Med. Image Comput. Comput. Assist. Intervention (MICCAI)*, Japan, 2002, pp. 216-223.

[9] L. Barbe, B. Bayle, M. de Mathelin, and A. Gangi, Needle Insertions Modeling: Identifiability and Limitations, *Biomed. Sig. Proc. Cont.*, vol. 2, pp. 191-198, 2007.

[10] R.J. Webster III, J.S. Kim, N.J. Cowan, G.S. Chirikjian, and A.M. Okamura, Nonholonomic Modeling of Needle Steering, *Int. J. Rob. Res.*, vol. 25, no. 5/6, pp. 509-525, 2006.

[11] C. Canudas De Wit, H. Olsson, K.J. Astrom, and P. Lischinsky, A New Model for Control of Systems with Friction, *IEEE Trans. Automat. Contr.*, vol. 40, pp. 419-425, 1995.

[12] C. Canudas De Wit, P. Tsiotras, E. Velenis, M. Basset, and G. Gissinger, Dynamic Friction Models for Road/Tire Longitudinal Interaction, *Veh. Syst. Dyn.*, vol. 39, no. 3, pp. 189-226, 2003.

[13] L.R. Ray, A. Ramasubramanian, and J. Townsend, Adaptive Friction Compensation Using Extended Kalman-Bucy Filter Friction Estimation, *Control Eng. Pract.*, vol. 9, pp. 169-179, 2001.

[14] P. Lichinsky, C. Canudas De Wit, and G.C. Morel, Friction Compensation for an Industrial Hydraulic Robot, *IEEE Control Syst. Mag.*, vol. 19, no. 1, pp. 25-32, 1999.

[15] M.R. Kermani, R.V. Patel, and M. Moallem, Friction Identification and Compensation in Robotic Manipulators, *IEEE Trans. Instrum. Meas.*, vol. 56, no. 6, pp. 2346-2353, 2006.

[16] S.P. DiMaio, S.E. Salcudean, "Needle Insertion Modelling and Simulation," *In Proc. of IEEE Int. Conf. on Rob. Autom. (ICRA)*, USA, 2002, vol. 2, pp. 2098-2105.

[17] H.S. Bassan, R.V. Patel, and M. Moallem, A Novel Manipulator for Percutaneous Needle Insertion: Design and Experimentation, *IEEE/ASME Trans. Mechatron.*, vol. 14, no. 6, pp. 746-761, 2009.